JOURNAL OF AIRCRAFT
Vol. 44, No. 1, January–February 2007

Computational Aeroelastic Analysis of Store-Induced Limit-Cycle Oscillation

Gregory H. Parker* and Raymond C. Maple†
Air Force Institute of Technology, Wright–Patterson AFB, Ohio 45433
and
Philip S. Beran‡
U.S. Air Force Research Laboratory, Wright–Patterson AFB, Ohio 45433

DOI: 10.2514/1.21051

Limit-cycle oscillation was simulated for a rectangular wing referred to as the Goland$^+$ wing. It was found that the aerodynamic nonlinearity responsible for limit-cycle oscillation in the Goland$^+$ wing was shock motion and the periodic appearance/disappearance of shocks. The Goland$^+$ structural model was such that in the transonic flutter dip region, the primary bending and twisting modes were in phase and coupled to produce a single-degree-of-freedom, torsional flutter mode about a point located ahead of the leading edge of the wing. It was determined that the combination of strong trailing-edge and lambda shocks which periodically appear/disappear, limited the energy flow into the structure. This mechanism quenched the growth of the flutter, resulting in a steady limit-cycle oscillation. Underwing and tip stores were added to the Goland$^+$ wing to determine how they affected limit-cycle oscillation. It was found that the aerodynamic forces on the store transferred additional energy into the structure increasing the amplitude of the limit-cycle oscillation. However, it was also found that the underwing store interfered with the airflow on the bottom of the wing, which limited the amplitude of the limit-cycle oscillation.

Nomenclature

C_L = coefficient of lift
C_M = coefficient of moment
c = chord
R = specific gas constant
x = streamwise position
z = vertical position
γ = ratio of specific heats
τ = thickness-to-chord ratio

I. Introduction

AIRCRAFT operating in the transonic region risk encountering limit-cycle oscillation (LCO), which is also called limit-cycle flutter and limited amplitude flutter [1]. LCOs are limited amplitude, self-sustaining oscillations produced by fluid-structure interactions. LCO results in undesirable airframe vibrations that adversely affect a pilot's ability to function and degrades targeting accuracy for fighter aircraft. Aircraft with high aspect ratio or highly swept wings can experience LCO [2].

LCO is related to flutter, which occurs when the dynamic pressure is increased to a critical value above which the system becomes dynamically unstable. When a nonlinear mechanism that counters the amplitude growth is present in this unstable region, LCO can result. The nonlinearity that sustains LCO can be in the structure, the aerodynamic flow, or in both. The case of interest for this study was the nonlinearity in the aerodynamic flow. Sources of aerodynamic nonlinearity include separated flow and shock motion in transonic flow [3].

Received 10 November 2005; revision received 21 August 2006; accepted for publication 22 October 2006.

*Major, USAF, currently assigned to Air Force Research Laboratory. AIAA Senior Member.
†Assistant Professor, Lt. Col., USAF. AIAA Senior Member.
‡Principal Research Aerospace Engineer, Multidisciplinary Technologies Center. AIAA Associate Fellow.

Tijdeman and Seebass [4] characterized the periodic motion of shock waves on oscillating airfoils into three different types. In type-A shock motion, the shock wave moves fore and aft sinusoidally. The shock strength may vary as the shock moves but the shock is always present [4]. In type-B shock motion, the shock moves sinusoidally as in type-A, but the shock disappears during a part of its backward motion [4]. Type-C shock motion occurs when a periodic shock wave leaves the airfoil and continues upstream as a weak, free shock wave [4]. Bendiksen [5] has shown that if a transonic flutter mode that appears to be a single-degree-of-freedom, torsional motion, ahead of the leading edge, has a phase angle between bending and torsion less than approximately 10 deg, and has a transition from a type-A to type-B shock motion, it is likely that LCO will result. This type-B shock motion limits the flow of energy from the fluid to the structure, resulting in LCO [5].

Underwing and tip stores can affect LCO by changing the inertial properties of the wing and by changing the aerodynamics of the wing. If a store mass is added forward of the elastic axis (EA), the flutter speed generally increases, which produces a stabilizing effect. If a store mass is added aft of the elastic axis, it has a destabilizing effect [6]. Exceptions to this can occur in the transonic flutter dip region [7]. For typical LCO, the amplitude is constant for a given flight speed. The amplitude increases when the flight speed is increased and a new constant amplitude is obtained when the flight speed is again fixed [1]. If the flight speed is decreased but is still above the flutter point, a new constant, lower amplitude is obtained. If the flight speed is decreased below the flutter point, the oscillations damp out. Therefore, if there is typical LCO at a given airspeed and a mass is added ahead of the elastic axis and it raises the flutter speed, the LCO amplitude will decrease because the given fixed airspeed becomes closer to the flutter speed. If the mass is moved aft of the elastic axis and it lowers the flutter speed, the LCO amplitudes will increase.

The role of store aerodynamics in LCO is less well understood. One can hypothesize two primary mechanisms by which store aerodynamics affect LCO: the stores could change or interfere with the airflow on the wing, thereby changing how the shock motion is limiting the energy transferred into the structure; and the store aerodynamic carriage loads that are transferred into the structure could sufficiently change the total forces experienced by the wing, thereby changing the LCO response. The first mechanism deals with

changes to the wing aerodynamics because of the presence of the store. The second mechanism is independent of any changes to the wing aerodynamics and any changes in the LCO are because of aerodynamic forces experienced by the store. The most likely method that store aerodynamics that affect LCO is through a combination of these two.

Advances in nonlinear modeling and computer hardware have led to nonlinear aeroelastic predictions for reasonably complex configurations [8–10]. However, there is continued interest in LCO motivated by the need to further understand the physics and mechanisms involved in LCO so that better LCO predictive tools can be developed [11]. This article examines the aerodynamic nonlinearities for a clean wing and the nonlinear aerodynamic effects induced by underwing stores. There have been several efforts where LCO driven by aerodynamic nonlinearities were studied [9,10,12]. This article adds to this knowledge base by providing a detailed analysis of the shock motion during LCO and by determining the role of store aerodynamics in LCO.

II. Aeroelastic Program

An aeroelastic analysis program based on a fluid solver, with a fully unstructured-grid formulation, capable of simulating flutter and LCO was successfully developed [13,14]. It was developed by integrating a modal structural model with the commercial computational fluid dynamics (CFD) fluid solver FLUENT 6.1, by FLUENT Incorporated. FLUENT 6.1 was chosen to fill the need for a solver that could rapidly and flexibly handle geometrically complex configurations undergoing structural deformation. A secondary goal of this research was to see if aeroelastic analysis of complex configurations was possible with a commercial CFD solver that would not require special knowledge of the analyst typically assumed by research codes. Any commercial solver chosen would require some modification before it could be used for aeroelastic analysis. FLUENT 6.1 was chosen because the required modifications seemed to be less complex than those required by other commercial codes that were considered. It was also chosen because it is a long established general purpose CFD solver with a deforming grid capability and multiple turbulence models available. FLUENT 6.1 is an unstructured Navier–Stokes fluid solver with a deforming grid capability that can be controlled through a user written subroutine called a user defined function (UDF). A UDF was written that coupled a modal structure model with force data from the fluid solver to compute structural deformations and deform the grid. The Newmark algorithm [15] was used to discretize the structural model and to solve for the displacements of the structural grid. The aeroelastic analysis program is fully parallelized to take advantage of using multiple processors. The fluid solver is second order accurate spatially and first order accurate temporally (when using the deforming mesh algorithms). The structural model is second order accurate, both spatially and temporally. Overall, the aeroelastic program is first order accurate in time. In general, the grid used by the structural model and the aerodynamic grid used by FLUENT, were nonpoint matching. A spline matrix was used to transfer data between the grids. Both the thin-plate spline [16–18] and infinite-plate spline [16,17,19] were implemented. Initial testing and validation of the code was completed on the Goland$^+$ and AGARD 445.6 wings [13,14]. In coupling FLUENT with a modal structure model, groundwork was laid to analyze aeroelastic problems for complex geometries.

The aeroelastic analysis program moves an attached store as a rigid body based on how the pylon attachment points move on the wing surface. The aerodynamic forces and moments acting on the store are calculated and transferred into the structure through the pylon, in order that any aerodynamic effects on the store are felt by the structural model. These forces can also be turned off or ignored, allowing the aerodynamic interference on the bottom of the wing due to the store to be isolated. To determine how much of an effect the store forces are having on LCO as compared with how much of an effect the store interference with the wing is having on LCO, the aeroelastic program can also magnify the store forces that are transferred into the structure. In addition, these magnified forces can be reversed in direction to further isolate their effect. The aeroelastic analysis program also allows for inertial forces to be added to the store aerodynamic forces. These forces are then transferred into the unchanged modal structural model.

III. Computational Experiment Setup

The Goland$^+$ wing was selected to study the impact of stores on LCO. This wing was chosen as a test case because data for ENS3DAE and CAPTSDv exist for this configuration [7,20]. The Goland$^+$ is a variant of the heavy Goland wing developed as a transonic flutter test case by Eastep and Olsen [21]. Based on the original Goland wing [22], the heavy Goland wing has increased mass to ensure applicability in the transonic region. The Goland$^+$ version of the heavy Goland wing was modeled with a box structure beam to allow a variety of store attachment options [7].

The Goland$^+$ wing is rectangular and cantilevered from an infinite midplane [7]. The wing semispan is 20 ft (6.096 m) and the chord is 6 ft (1.8288 m). The thickness τ is 0.04 ft (0.01219 m). The elastic axis is located 2 ft (0.6096 m) from the leading edge. The airfoil section is constant over the spanwise extent of the wing and is a symmetric, parabolic-arc airfoil given by

$$z = \pm 2\tau\left(1 - \frac{x}{c}\right)\left(\frac{x}{c}\right) \tag{1}$$

The Goland$^+$ is known to exhibit LCO when a tip mass of 22.498 slugs (328.3313 kg) and a rotational inertia of 50.3396 slugs-ft^2 (68.2509 kg-m^2) is located 1.75 ft (0.5334 m) forward of the elastic axis [7]. Natural vibration modes for the Goland$^+$ wing with a tip mass were obtained from MSC/NASTRAN [7]. The first six modes were used in the aeroelastic analysis. The modes are plotted in Fig. 1, which shows the top of the right wing with the leading edge to the upper right and the trailing edge to the lower left.

The Goland$^+$ simulations were started by giving mode 2 a modal displacement perturbation of 0.02. These results were then compared to the results presented by Snyder et al. [20]. At 600 ft/s (182.88 m/s) and Mach 0.92, the dynamic pressure is beyond the flutter point and was shown by Snyder et al. [20] to result in LCO. For the Goland$^+$, these flow conditions fall within the transonic flutter dip region. This case was used as a baseline for all simulations in this study. Snyder et al. [20] used non-match-point flow conditions for their analysis. For each test case, they chose a Mach number and velocity and fixed the far-field density and temperature values at standard-day, sea-level conditions. This resulted in nonphysical conditions. FLUENT normally requires physical (matched-point) conditions. To match their flow parameters, the specific gas constant R and the far-field pressure were varied for different Mach number and velocity settings. The specific heat ratio γ was held fixed at 1.4. To match the conditions of Snyder et al. [20] for Mach 0.92 and 600 ft/s (182.88 m/s), the far-field density, temperature, and pressure were set to 0.0023771 slugs/ft^3 (1.225 kg/m^3), 518.67°R (288.15 K), and 722.1813 lb/ft^2 (34,578.04 Pa), respectively, while R was set to 585.7438 ft · lb$_f$/slug · °R ($R = 97.951$ N · m/Kg · K).

All of the Goland$^+$ simulations used a time step of 0.001 s corresponding to approximately 300 time steps per cycle. To check for time-step convergence, a time step of 0.0005 was tested. Cutting the time step in half changed the mode 1 response by 0.367%, the mode 2 response by 0.027%, the coefficient-of-lift (C_L) response by 0.029%, and the frequency by 0.160%. These changes were sufficiently small that the time step of 0.001 s was considered converged.

To test grid convergence, an aerodynamically clean, Goland$^+$ wing configuration was run on three different inviscid grids. A coarse grid of 68,949 tetrahedral cells with 518 cell faces on the wing, a medium grid with 194,780 tetrahedral cells with 9178 cell faces on the wing, and a fine grid with 269,596 tetrahedral cells with 13,358 cell faces on the wing were used. All of the grids correctly

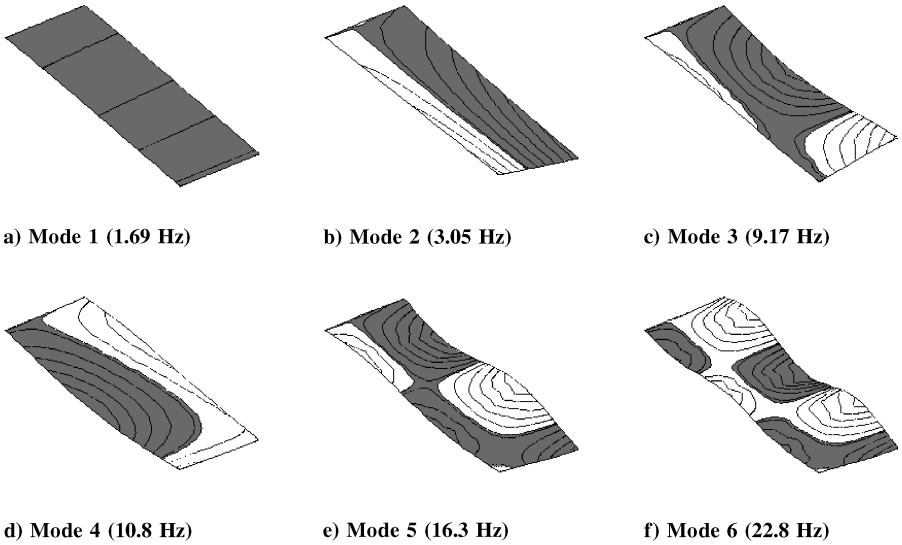

a) Mode 1 (1.69 Hz) b) Mode 2 (3.05 Hz) c) Mode 3 (9.17 Hz)

d) Mode 4 (10.8 Hz) e) Mode 5 (16.3 Hz) f) Mode 6 (22.8 Hz)

Fig. 1 Mode shapes for the Goland$^+$ wing with tip store.

captured the LCO, including the coarse grid. This was initially surprising, because the coarse grid did not accurately capture the pressure distribution on the wing at the leading and trailing edges, nor did it accurately define the shock location because of the large size of the cells. However, because the structural grid was coarser than even the coarse aerodynamic grid and the spline conserved the forces by lumping the forces at the nodes, all of the aerodynamic grids produced a similar force distribution when transferred to the structural grid. The amplitudes of the LCO and the modal contributions were approximately the same regardless of the grid. The only variation in the LCO because of grid refinement was the frequency. The frequency was 3.37 Hz for the coarse grid, 3.31 Hz for the medium grid, and 3.27 Hz for the fine grid.

To determine the role store aerodynamics plays in LCO, grids for various store configurations were created and used with the same structural model used by the clean wing. Therefore, in these cases, the stores were modeled aerodynamically but not structurally. The tip mass was retained in the structural model because it was necessary for the clean wing to obtain LCO. The grids were created by starting with the clean grid of 68,949 tetrahedral cells with 518 cell faces on the wing, and then adding store shapes.

Underwing and tip stores were added to the Goland$^+$ wing and the same initial perturbation and boundary conditions were used as that studied for the clean wing. Underwing stores can be added to the Goland$^+$ wing at any rib station. These stations are evenly spaced 2 ft (0.6096 m) apart. Aerodynamic forces and moments were calculated for the store at the point the pylon joined the wing on the elastic axis. These forces and moments were transferred into the structural model at this point. Underwing stores were added at 20% [4 ft (1.2192 m)], 50% [10 ft (3.048 m)], and 80% [16 ft (4.8768 m)] half-span. The underwing configurations consisted of the Goland$^+$ grid with a 10 ft (3.048 m) long, 12 in. (0.3048 m) diameter cylindrical store with an elliptic nose cone centered below the wing. The top of the store was located 12 in. (0.3048 m) below the bottom of the wing and was attached to the wing via a biconvex-shaped pylon that was 3 ft (0.9144 m) long centered chordwise under the wing. The grid with a tip store consisted of the Goland$^+$ grid with a 10 ft (3.048 m) long, 5 in. (0.127 m) diameter cylindrical store with an elliptic nose cone centered on the wing tip. Store and pylon dimensions were selected based on typical stores in United States Air Force inventory. The 20% half-span underwing store and the tip-store configurations are shown in Fig. 2.

Additional store configurations were also analyzed to determine how store modifications change the store forces or change the interference on the bottom of the wing. Over 60 different configurations were analyzed. Initially, fins were added to the stores and the pylon height was shortened both for stores with and without fins. Next, the baseline stores were moved fore and aft. Store diameter was then increased and finally, multiple stores were added to the wing. The effect fins had on LCO was examined by adding fins to the tail of the stores for the four store configurations. The pylon height effect was studied by changing the height from 12 in. (0.3048 m) to 6 in. (0.1524 m). The effect of streamwise positioning of the store was examined by modifying the position of the underwing store grids by shifting the stores 2 ft (0.6096 m) fore and aft, while the 12 in. (0.3048 m) pylon remained centered beneath the wing. The effect store diameter had on LCO was examined by doubling the underwing store diameter to 24 in. (0.6096 m) and the tip-store diameter to 10 in. (0.254 m). Finally, multiple, small-diameter stores were added to the Goland$^+$ wing to create further interference on the bottom of the wing. The tip store and the underwing stores at 20 and 50% half-span were added to the Goland$^+$ wing. This was repeated for the large-diameter stores.

Inertial forces were added to the stores to determine the relative importance of store aerodynamics versus store mass. The structural model was not modified. Instead, the inertial forces were calculated by assuming a mass of 25 slugs (364.8476 kg) was located a fixed distance from the elastic axis. These forces were combined with the store aerodynamic forces and fed through the pylon into the wing structure. The configurations with a 12 in. (0.3048 m) diameter

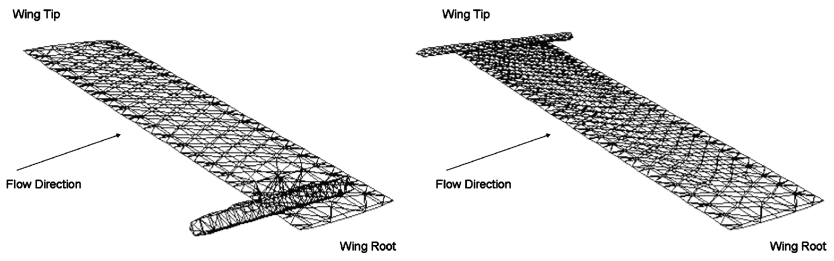

a) Underwing Store at 20% Half-span b) Tip Store

Fig. 2 Goland$^+$ wing with aerodynamic stores surface grids.

underwing store centered on a 12 in. (0.3048 m) pylon and the 5 in. (0.127 m) diameter tip store were run with a store mass located −2 ft (−0.6096 m), −1 ft (−0.3048 m), 0 ft (0.0 m), 1 ft (0.3048 m), and 2 ft (0.6096 m) in the x direction (streamwise direction) from the elastic axis.

IV. Clean Goland$^+$ Wing Results

The LCO for the Goland$^+$ clean-wing configuration consisted of a nearly in-phase coupling of mode 1 and mode 2 which produced a single-degree-of-freedom, torsional motion, with an axis of rotation running from the elastic axis at the wing root to a point slightly forward of the leading edge at the wing tip. The LCO had an amplitude of ±1.065 for C_L, ±0.47 for the coefficient of moment (C_M), and ±20.6 deg for the tip angle of attack. The two dominant modes had an amplitude of ±8.8 for mode 1 and ±7.5 for mode 2 (Fig. 3). The amplitude of mode 3 was ±0.66 which was only 7.5% of the contribution of mode 1. The remaining modes contributed even less. A power-spectral-density plot of the motion showed that the power was primarily at 3.3 and 9.8 Hz with some contribution from 6.5 and 10.7 Hz. The dominant modes in the LCO response were mode 1 followed closely by mode 2. However, the dominant forces were mode 1 followed by mode 4. The remaining force contribution was in mode 3, mode 5, then finally mode 2 and mode 6. These modal forces were determined by multiplying the transpose of the modal matrix by the vector of forces on the structural grid.

The wing tip experienced a large angle of attack, therefore, steady inviscid and viscous solutions were calculated for angles of attack up to 20 deg to verify that the flow remained attached to the wing and that there was no separation. There was also no structural nonlinearity included in the structural model. Therefore, the only nonlinearity present was due to the presence and movement of shocks. The shock was initially located at approximately 80% chord where it ran from the wing root, to the wing tip, with a slight curve forward before disappearing at the wing tip (Fig. 4). As the wing began to deform, the shock started to slowly move fore and aft sinusoidally (type-A shock motion [4]). As the amplitude of the wing motion increased, the magnitude of the shock strength changed periodically with the motion until the shock disappeared during part of its aft motion (type-B shock motion [4]). Transition from type-A to type-B was observed at approximately 2.9 s, ranging from the wing root to about 50% span. The shock motion for the outboard 50% span remained type-A. The inboard type-B shock motion limited the energy flow and changed the mode 1 amplitude growth from an exponential growth to a linear growth, as seen in Fig. 3. This type-B motion continued to gain strength until it consisted of an appearing and disappearing shock at the trailing edge with no observable fore/aft motion. However, this type-B shock motion was only on the inboard 50% span. Most of the energy flowing into the structure was occurring on the outboard 50% span. At approximately 4.6 s, a periodic, lambda shock began to appear and disappear near the wing tip in conjunction with a strong, normal shock moving fore and aft at the trailing edge. This lambda shock and normal shock further limited the energy transferred from the fluid to the structure. At 6.4 s, the wing was in LCO. The combination of type-B shock motion, lambda shock motion, and trailing-edge normal-shock motion were responsible for quenching the energy flow from the fluid to the structure resulting in LCO for this wing.

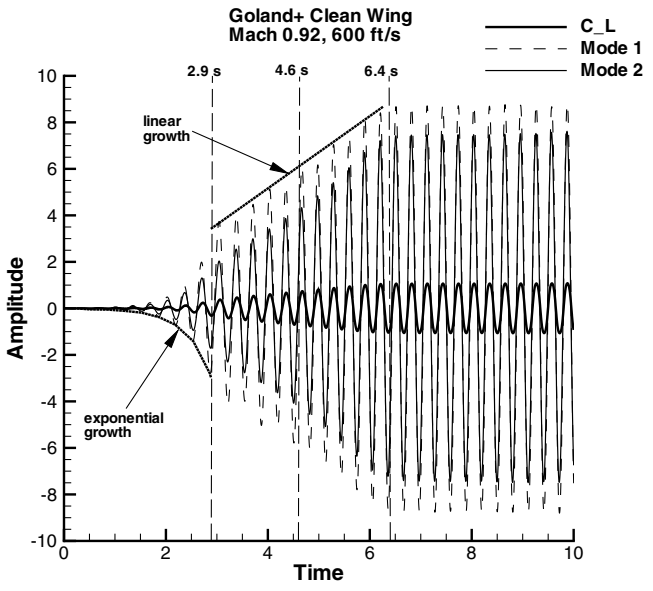

Fig. 3 Clean wing C_L and modal amplitudes.

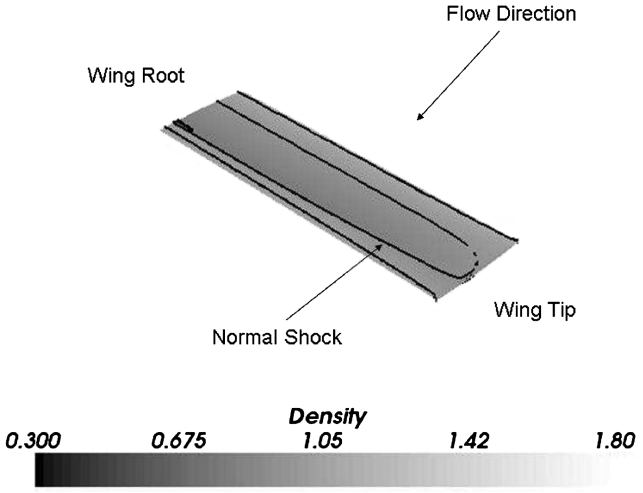

Fig. 4 Steady-state density contours.

The coupling of mode 1 and mode 2 into a single-degree-of-freedom, torsional motion, about a point ahead of the leading edge, leads to a wing twisting motion such that the aerodynamic forces on the wing are constantly pushing the wing toward the static aeroelastic position. When the wing bends down and twists up, the aerodynamic forces try to restore the wing to its static aeroelastic position. However, the restoring forces are large enough that the amount of energy transferred into the wing causes the wing to overshoot its neutral point, bending and twisting even further in the opposite direction, leading to a growing oscillation. When the oscillations grow to the point that the trailing-edge shock and lambda shock appear near the wing tip, the shocks limit the force on the wing, thereby limiting the overshoot. When the shock strength reaches the point that it balances the inertial forces, a stable LCO is achieved. Figure 5 illustrates the pressure distribution on the wing. If the normal shock and lambda shock were not present, the pressure on the top of the wing would be lower, so that the net force on the wing would be higher leading to the wing bending and twisting further in each subsequent cycle.

During a LCO cycle (Fig. 6), the wing starts bending down and twisting up. A normal shock appears near the trailing edge on the outboard portion of the wing (Fig. 6a). This normal shock begins to limit the flow of energy from the fluid into the wing. As the wing continues to bend down and twist up, a lambda shock appears near the tip (Fig. 6b). When the lambda shock first appears, it runs from the leading edge of the wing near the tip to where the trailing-edge normal shock meets the trailing edge near 50% span. As the wing continues to bend down and twist up, the lambda shock strengthens and the shock angle increases. At the extreme of the wing motion, the lambda shock runs from the leading edge of the wing near the tip, to the center of the normal shock at the trailing edge, at approximately 75% span (Fig. 6c). As the wing then begins to straighten and untwist, the lambda shock reverses direction and the shock angle begins to decrease. The normal shock at the trailing edge also begins to weaken and move aft (Fig. 6d). At the end of the first half of the LCO cycle, the shocks are completely gone and the forces on the top and bottom of the wing are nearly balanced (Fig. 6e). This is repeated for the second half of the LCO cycle when the wing starts to bend up and twist down.

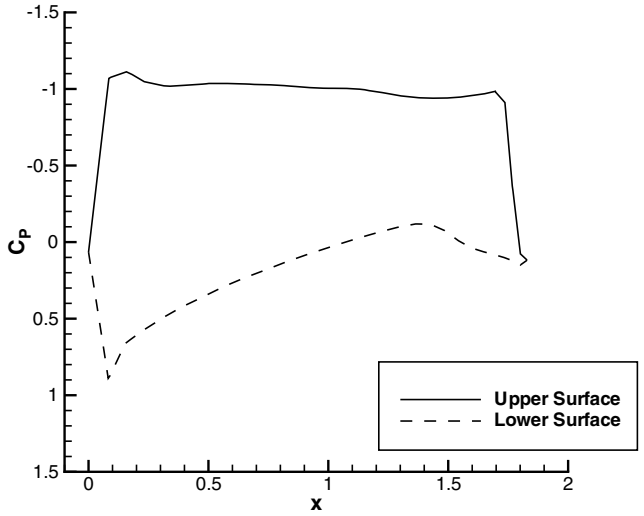

a) 3m span

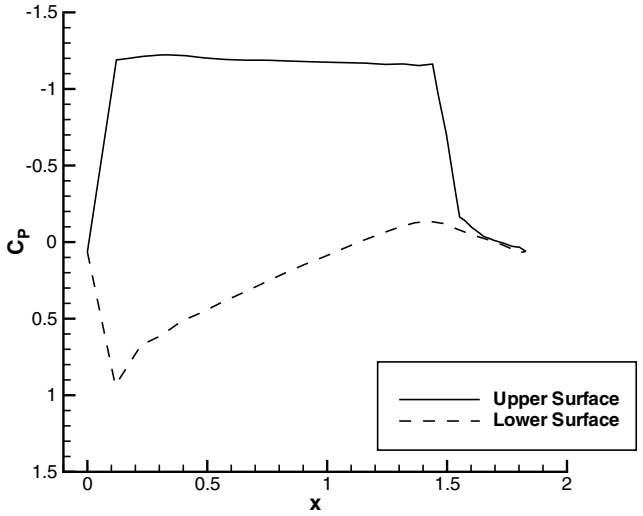

b) 4m span

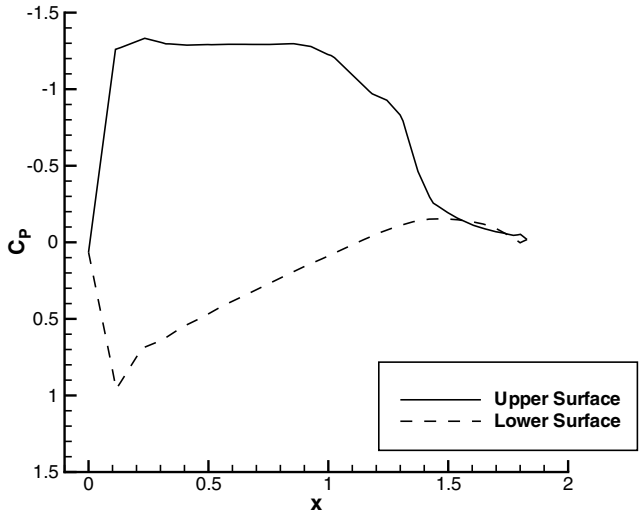

c) 5m span

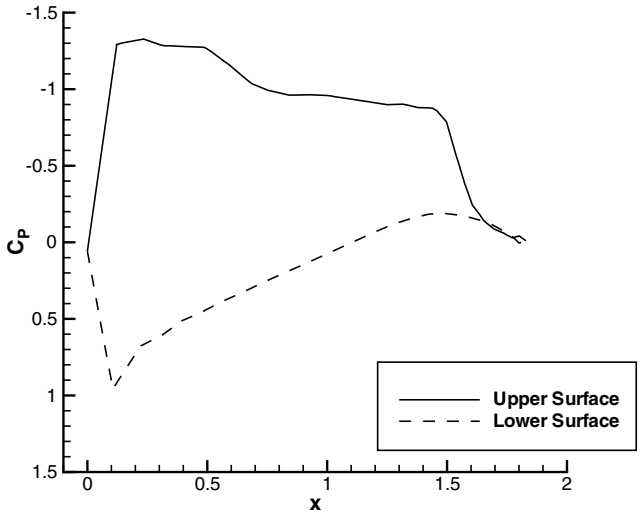

d) 5.5m span

Fig. 5 Clean wing at 6.815 s (pressure distribution).

Figure 7 shows the steady pressure contours for a rigid wing at 20 deg angle of attack. The forces on the rigid-wing airfoil section are much higher than those shown in Fig. 5d, even though the angle of attack at the tip is approximately the same. This difference in force is because of the shocks, which provide the quenching mechanism responsible for LCO in this wing. The normal shock and lambda shock do not appear if the wing is given a constant angle of attack. However, if the wing is deformed into the bent and twisted shape that occurs during LCO, and a steady-state flow solution is computed, the lambda and trailing-edge shocks are present. These shocks are present because of the shape of the wing and not because of the dynamic motion of the wing. The dynamic motion does, however, play a role in the shock strength and movement. The shocks are weaker and slightly aft when computed for steady-state flow versus those computed for dynamic motion. The coupling of the primary bending and twisting modes is what leads to this deformed shape, which in turn leads to shock motion that provides the energy quenching necessary for LCO.

If a wing is undergoing LCO, a phase plot will trace an orbit along a closed path and there will be zero net work over a cycle [5]. For the clean-wing configuration, the point where the elastic axis intersects the wing tip was plotted for plunge rate versus plunge. This plunge phase plot, shown in Fig. 8a, shows the growth of the amplitudes culminating in a closed path indicating LCO. The pitch rate of the wing tip was also plotted versus pitch. This pitch phase plot, shown in Fig. 8b, also shows the growth of the amplitudes culminating in LCO.

To determine whether the angle of attack of the wing affects the flow of energy between the fluid and the structure, the root angle of attack was changed from 0.0 to 2.0 deg. Changing the angle of attack changed the static aeroelastic solution, causing a displacement of the static values about which the modes and C_L oscillated. The wing oscillated about a C_L of 0.1676 instead of 0.0 and about a tip angle of attack of 1.36 deg instead of 0.0 deg. This new neutral point was the new static aeroelastic solution for the wing at 2.0 deg angle of attack. The pattern of the energy flow between the fluid and the structure was unaffected.

V. Goland$^+$ Wing with Underwing Stores Results

One of the goals of this study was to determine the role of store aerodynamics in LCO. It was found that aerodynamic store shapes affect LCO in two offsetting ways: by interfering with the flowfield on the wing surface, and by transferring additional store forces into

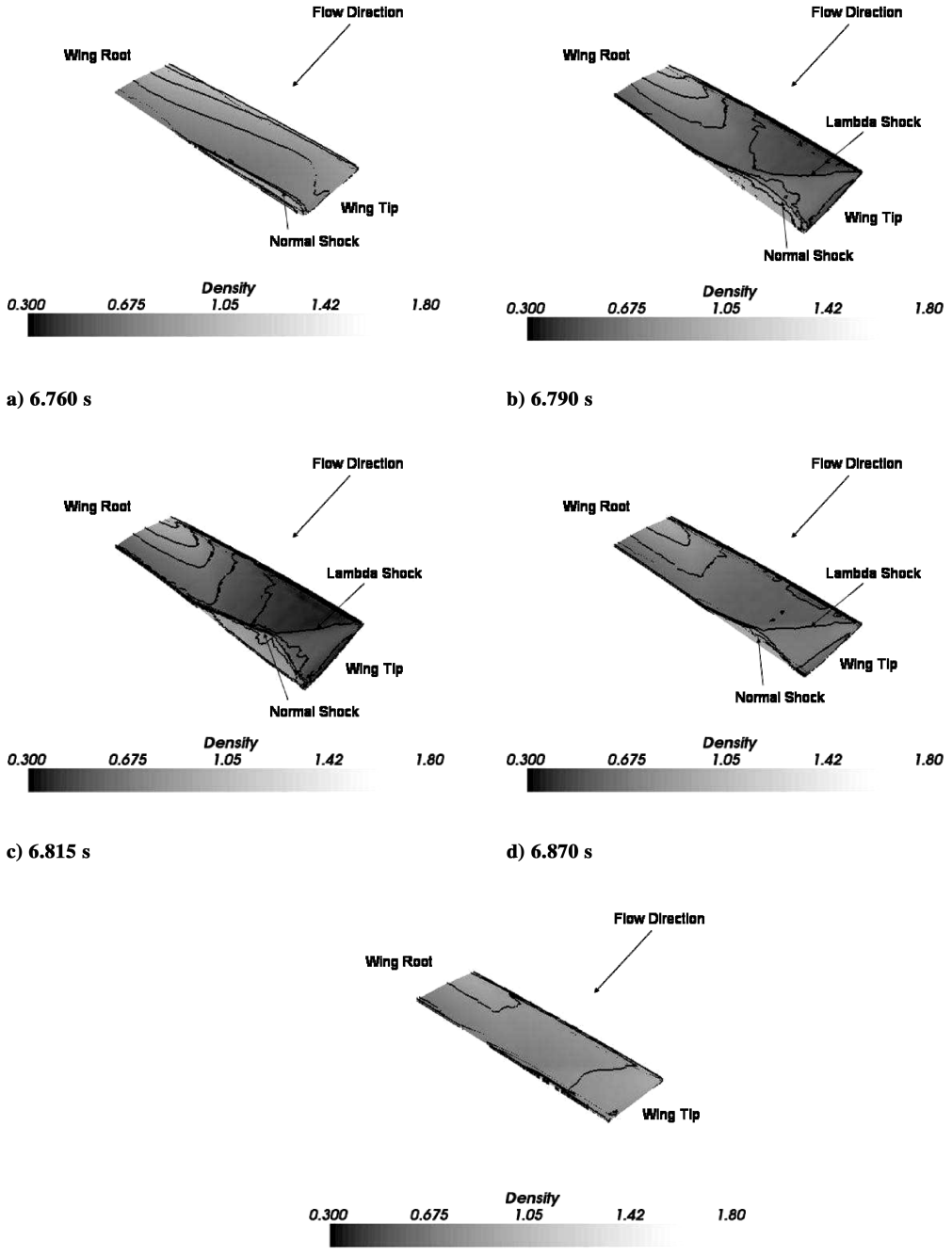

Fig. 6 Clean wing (density contours).

the structure. The underwing stores interfere with the airflow on the lower surface of the wing which decreases LCO amplitudes, whereas, store forces transferred into the wing structure directly increase LCO amplitudes.

The outboard section of the wing experienced greater bending and twisting deformation than the inboard section of the wing. This greater deformation meant that stores had a greater impact on LCO the further outboard they were placed. An exception to this was found at the 50% half-span location. Small stores with the 12 in. (0.3048 m) pylon were placed at 20, 50, and 80% half-span locations as discussed in Sec. III. Adding stores increased the mode 2 response in all cases. The mode 1 response decreased for stores at 20 and 80% half-span and increased for stores at 50%. It was speculated that this increase was because of the mode 3 mode shape (Fig. 1) which had large displacements in the middle of the wing. Further weight was added to this speculation by observing that the stores primarily contributed to mode 3 forces implying that the store located where mode 3 provided the greatest deformation had the greatest effect. It appears that the aerodynamics are coupling the modes and that energy added into the structure through mode 3 is being transferred into modes 1 and 2. Adding the underwing stores increased the magnitude of the total modal forces, the magnitude of C_L, and the magnitude of the tip angle of attack. These changes resulted in LCO being reached more quickly than with a clean wing.

For the 20 and 80% half-span configurations, the stores only contributed 0.2% of the peak force in mode 3. The 50% store contributed 0.7% of the peak force in mode 3. To increase these store forces, fins were added to the tail of all the store configurations. The fins were aft of the wing so that they did not affect the flowfield on the wing. For these small stores, fins did not make a difference in the

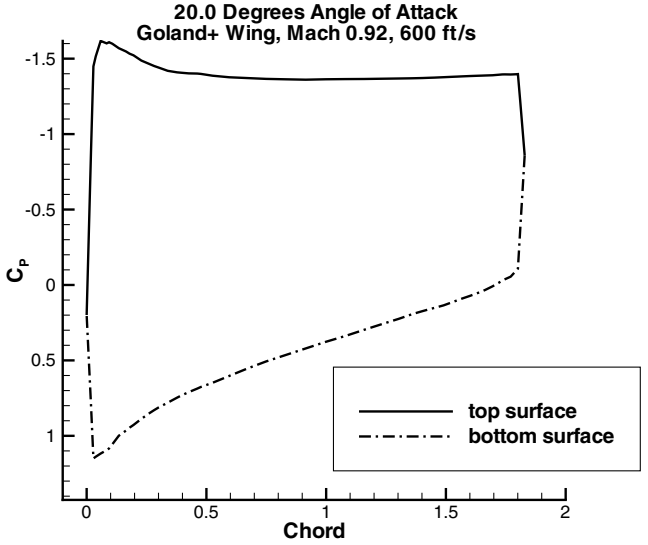

Fig. 7 Rigid-wing airfoil C_P plot for 20 deg angle of attack.

LCO behavior. They did increase the store forces, but the store forces were so small compared to the wing forces that the effects on LCO were negligible. The pylon height was changed from 12 in. (0.3048 m) to 6 in. (0.1524 m) in order to change the store moments. Shortening the pylon only made a small difference in the LCO behavior. The store forces and the wing response were similar, regardless of the pylon height. Shortening the pylon led to lower mode 2 amplitudes, or less twist, but otherwise, the behavior was the same regardless of pylon height. The fins and pylon height weakly affected the twisting moment, whereas, the bending force was the primary contributor to LCO.

The store forces that were transferred into the structural model were magnified to amplify how the store forces affected the LCO. Solutions for the wing with a 12 in. (0.3048 m) diameter underwing store centered on a 12 in. (0.3048 m) pylon were computed, but with the store forces that were calculated from the aerodynamic loads being magnified by ± 5 before being transferred into the structural model. Altering the store forces in this manner affected the LCO (Fig. 9). The store forces increased the total bending force on the wing, which increased the LCO amplitude. The bending force primarily affected LCO by directly contributing to mode 1. Magnifying the bending force increased the amplitude of the LCO because it increased the restoring force, resulting in greater overshoot beyond the neutral position. Magnifying and reversing the phase of the loads (multiplying forces by -5) decreased the restoring force resulting in less overshoot and a decreased amplitude LCO. These results reinforced the hypothesis that the increased LCO amplitudes observed with small underwing stores were caused by the store loads which were greater than the quenching effect caused by interference of the flow on the bottom of the wing.

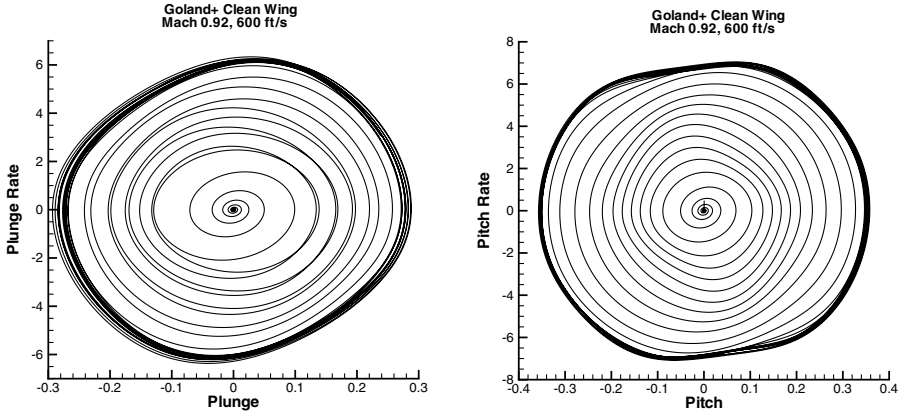

a) Plunge Phase Plot (Wing Tip) **b) Pitch Phase Plot (Wing Tip)**

Fig. 8 Clean-wing phase plots.

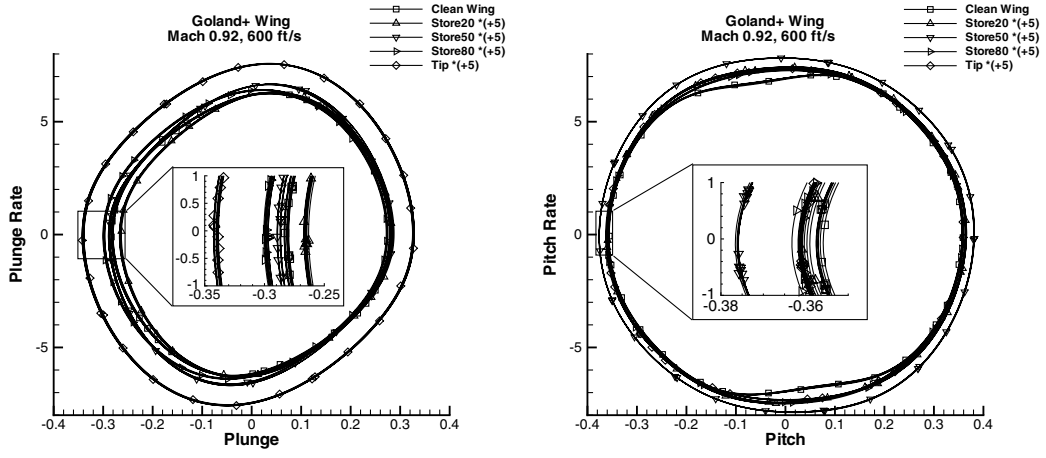

a) Plunge Phase Plot (Wing Tip) **b) Pitch Phase Plot (Wing Tip)**

Fig. 9 Phase plots when store forces are magnified by +5.

The second mechanism by which underwing stores affected LCO was by interfering with the airflow on the bottom of the wing. The 80% half-span configuration with a small store was computed with the store forces turned off in order to isolate this interference effect. The only difference between the clean wing and this computation was interference from the store. When the store forces were ignored, C_L decreased 0.97%, C_M decreased 1.26%, the tip angle of attack decreased 1.59%, mode 1 amplitudes decreased 1.67%, and mode 2 amplitudes decreased 1.82% when compared to the clean-wing configuration. These results showed that the LCO amplitudes decreased and demonstrated the damping provided by store interference.

The underwing store grids with the 12 in. (0.3048 m) pylon and fins were modified to see how streamwise store position affects the interference on the bottom of the wing. The stores were shifted 2 ft (0.6096 m) fore and aft. The pylon remained centered beneath the wing. Moving the store aft produced LCO. When the 50% half-span store and the 80% half-span store were moved forward, the flow separated on the store causing the inviscid fluid solver to fail, so no conclusions could be drawn. The 20% half-span store resulted in LCO when moved forward. This LCO magnitude was similar to the original centered store position. When the stores were moved aft, they only slightly affected the LCO. Shifting underwing stores fore or aft only slightly changed the LCO because the change in the forces was very small and the interference of the flow on the wing because of the store remained small.

To further amplify the interference effect, the stores without fins were doubled in diameter to 24 in. (0.6096 m). The centered 12 in. (0.3048 m) pylon was retained. As can be seen in Fig. 10, the large-diameter store had a large affect on the LCO, whereas adding a small underwing store produced an LCO of slightly greater amplitude, adding a large underwing store resulted in an LCO of smaller amplitude. The further outboard the large store, the smaller the amplitude of the LCO. Again, the total modal forces did not change greatly for large stores. The aerodynamic forces were slightly higher with a large store than with a small store but were still less than 1% of the total forces for all modes. This indicated that the large store was affecting the flow on the bottom of the wing and it was influencing the dynamic shock motion which was limiting the energy flow into the structure. The interference effect was not great enough to damp out the oscillations, but it was enough to decrease the LCO amplitude.

The large store at 80% half-span illustrates how underwing stores affect the flowfield on the bottom of the wing, and thereby, affect the LCO. When the wing was bent up and twisted down, the flow on the top of the wing was unchanged from the clean-wing condition. However, on the bottom of the wing (Fig. 11a) there were significant changes when compared to the clean wing at the same point in an LCO cycle (Fig. 11b). The lambda shock was weak if detectable at all, and the normal shock at the trailing edge was weaker than that experienced by the clean wing. The store wake, or the flow from the store that impinged on the flow on the bottom of the wing, increased the pressure on the front half of the wing in the vicinity of the store. The normal shock then increased the pressure again (Fig. 12). The increase in pressure decreased the downward restoring force on the wing, which had the same effect as the lambda shock on the clean

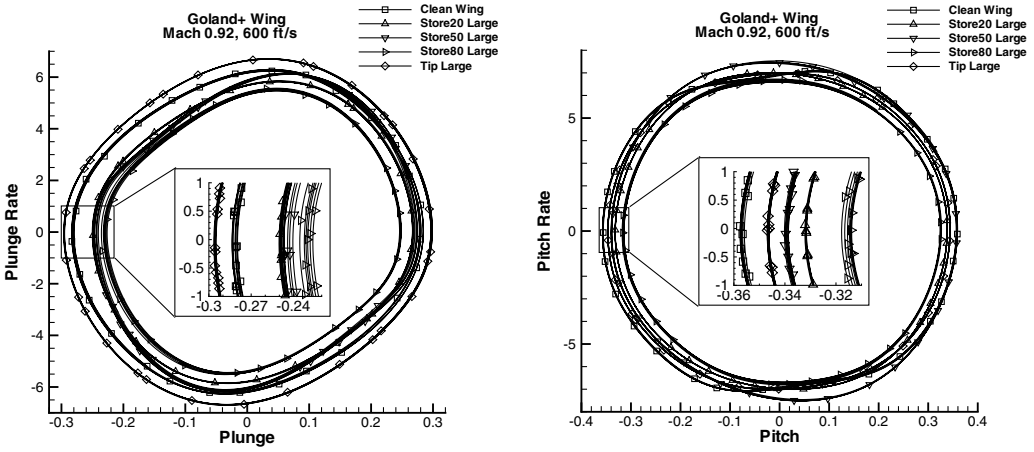

a) Plunge Phase Plot (Wing Tip) **b) Pitch Phase Plot (Wing Tip)**

Fig. 10 Phase plots for large stores.

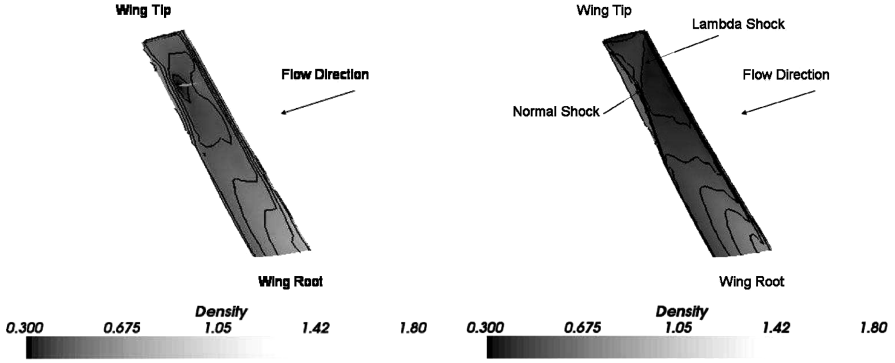

a) Large 80% Store **b) Clean Wing**

Fig. 11 Large 80% store at 10.495 s (density contours).

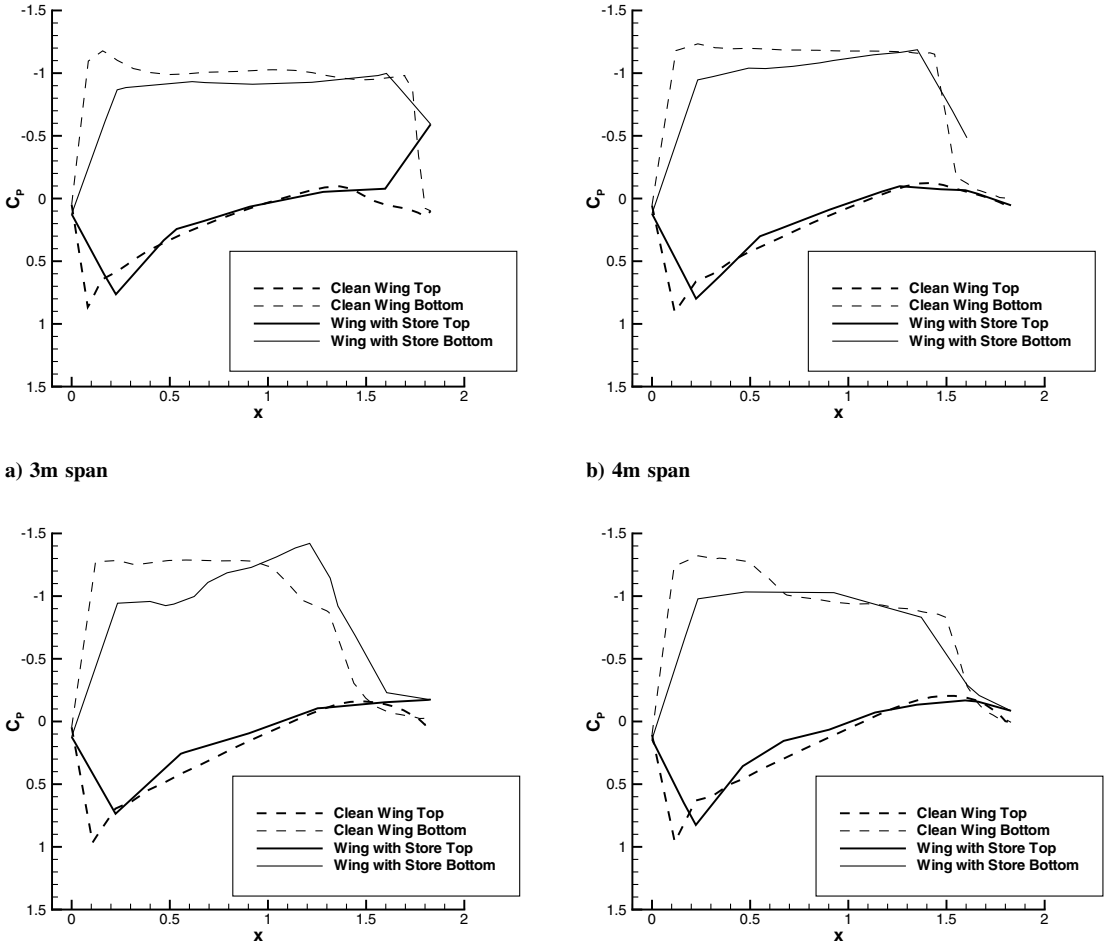

a) 3m span

b) 4m span

c) 5m span

d) 5.5m span

Fig. 12 Large 80% store at 10.495 s (pressure distribution).

wing, limiting the energy flow into the wing. When the wing was bent down and twisted up, the flow on the top of the wing was unchanged from the clean-wing condition. The lambda shock and trailing-edge shock were present, though weaker than those present in the clean wing because of the lower pitch and plunge amplitudes. These shocks were still providing quenching leading to LCO. If the store was large enough to have a large wake raise the pressure on the wing, it provided quenching. A very small store with a minimal wake had minimal impact on the LCO caused by interference from the store.

Multiple, small-diameter stores were added to the Goland$^+$ wing to create further interference. A tip store and the underwing stores at 20 and 50% half-span were added to the Goland$^+$ wing. The centered 12 in. (0.3048 m) pylon was retained. The small-diameter stores resulted in an LCO with an amplitude slightly greater than the clean wing. For the small stores, the store forces effect was stronger than the interference damping effect. Multiple, large-diameter stores were then added to the Goland$^+$ wing to create further interference. When the large-store configuration was run, the oscillations damped out. The multiple, large stores interfered with the flow on the bottom of the wing to the extent that it prevented the energy flow into the structure, resulting in damping.

One effect that underwing stores had on LCO was shown by the mode 1 response oscillating about a negative value instead of about zero, as with a clean wing or with a tip store. This showed that the presence of the underwing stores shifted the static aeroelastic solution. Shifting the static aeroelastic solution did not change the LCO response, only the neutral configuration about which the wing oscillated.

To examine the effect of store mass position on LCO as opposed to the store aerodynamics, inertial forces were added to the store aerodynamic forces. The 12 in. (0.3048 m) diameter underwing stores centered on 12 in. (0.3048 m) pylons were run with a store mass located −2 ft (−0.6096 m), −1 ft (−0.3048 m), 0 ft (0.0 m), 1 ft (0.3048 m), and 2 ft (0.6096 m) in the x direction (streamwise direction) from the elastic axis. When the mass was added on the elastic axis or forward of the elastic axis, the LCO amplitude only slightly increased for the underwing store located at 20% half-span. However, if the mass was added 1 ft (0.3048 m) aft of the elastic axis, a different LCO mode was encountered (Fig. 13). The amplitudes grew in the same manner as the case without the mass, but at approximately 4 s, mode 4 started growing and eventually stabilized. At approximately 14 s, a new LCO state was reached. When the mass was added 2 ft (0.6096 m) aft of the elastic axis, all of the modes grew, leading to divergent flutter.

When the mass was added to the 50% half-span, underwing store, divergent flutter was obtained for all streamwise locations. It was hypothesized that this was because the stores primarily contributed to mode 3 forces. As discussed earlier, due to the aerodynamic coupling, when the store was located where mode 3 provided the greatest contribution, it had a larger effect on the LCO amplitude than expected. Adding additional inertia forces through this point by placing a mass at 50% half-span thereby increasing the mode 3 forces even more, had a very large effect. When the mass was placed on the elastic axis, it came close to stabilizing into an LCO. It initially appeared to enter the LCO condition observed without the mass, but at approximately 6 s, mode 4 started to diverge followed by mode 3 and the remaining modes, eventually driving the system to divergent flutter (Fig. 14). For the other 50% half-span mass locations, all the modes went unstable and the system immediately went into divergent flutter.

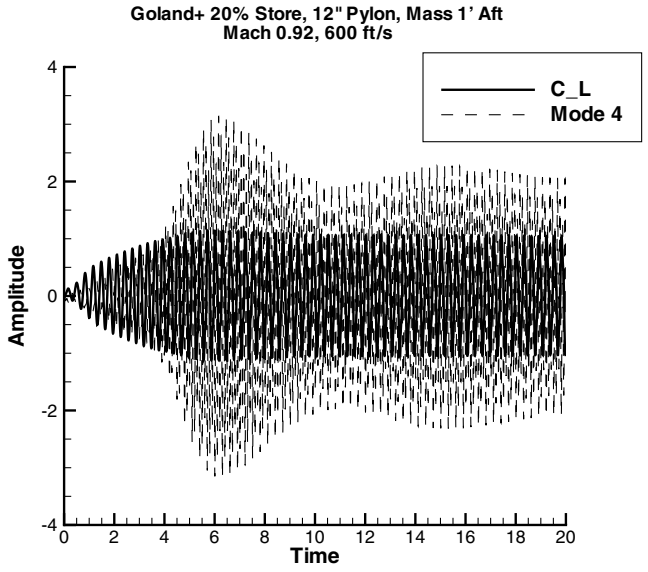

Fig. 13 Amplitudes for point mass 1′ aft of EA at 20% half-span.

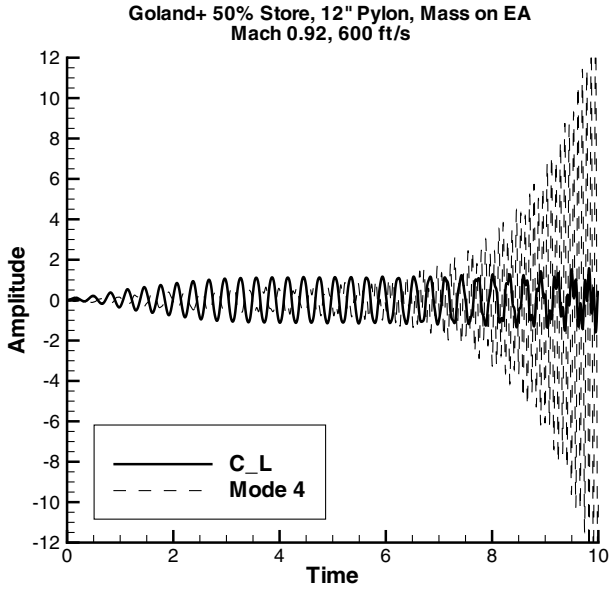

Fig. 14 Amplitudes for point mass on EA at 50% half-span.

Providing mass to the 80% half-span store at different chordwise locations illustrated the stabilizing and destabilizing effects of mass position, as shown in Fig. 15. When the mass was located on the elastic axis, a LCO response similar to the no-mass case was observed. As the mass was moved forward of the elastic axis, LCO amplitudes decreased drastically, mode 2 increased in dominance, and mode 1 decreased in significance. This result was expected because adding a mass forward of the elastic axis generally raises the flutter speed, thereby decreasing LCO amplitude. The modes continued to be coupled into a single-degree-of-freedom response. When the mass was moved aft of the elastic axis, LCO amplitudes increased significantly. Again, this matched the expected result because adding a mass aft of the elastic axis generally lowers the flutter speed, leading to an LCO of increased amplitude. Mode 1 continued to grow in dominance while mode 2 decreased in importance. The modes continued to be coupled into a single-degree-of-freedom response, but with mode 4 growing and beginning to play a role in the response. However, by the time the mass had moved 2 ft (0.6096 m) aft, it was no longer a single-degree-of-freedom response, and a different LCO state was reached. If the mass continued to move aft, mode 4 would begin to dominate and divergent flutter would be encountered.

Adding inertial forces had a larger effect on the aeroelastic response than adding store aerodynamics. This can be seen in Fig. 15a. Adding the 80% half-span underwing store aerodynamics decreased the tip plunge by 3.8%. Adding inertia forces for a mass 1 ft (0.3048 m) forward of the elastic axis, in addition to the store aerodynamic forces, decreased the tip plunge an additional 22.5% while 2 ft (0.6096 m) forward decreased the tip plunge an additional 72.5%. Adding inertia forces on the elastic axis increased the tip plunge by 26.5% while adding inertia forces 1 ft (0.3048 m) and 2 ft (0.6096 m) aft of the elastic axis increased the tip plunge by 72.5% and 117.6%, respectively.

Adding inertial forces did not change the shock motion nor change the quenching mechanism. It did change the inertia of the wing and determined how efficient the shock motion was at limiting the energy transferred into the structure. Moving the mass forward increased the distance between the wing section center of gravity and the wing section aerodynamic center, thereby increasing the twisting moment on the section increasing twist, and generating greater shock motion. This caused the energy flow to be limited before the inertia grew too high, decreasing the LCO amplitude. Conversely, moving the mass rearward decreased the distance between the wing section center of gravity and the wing section aerodynamic center, decreasing the twisting moment on the section, decreasing twist and increasing bending. This allowed the inertia to grow higher before the shock motion limited the energy flow, increasing the amplitude of the LCO.

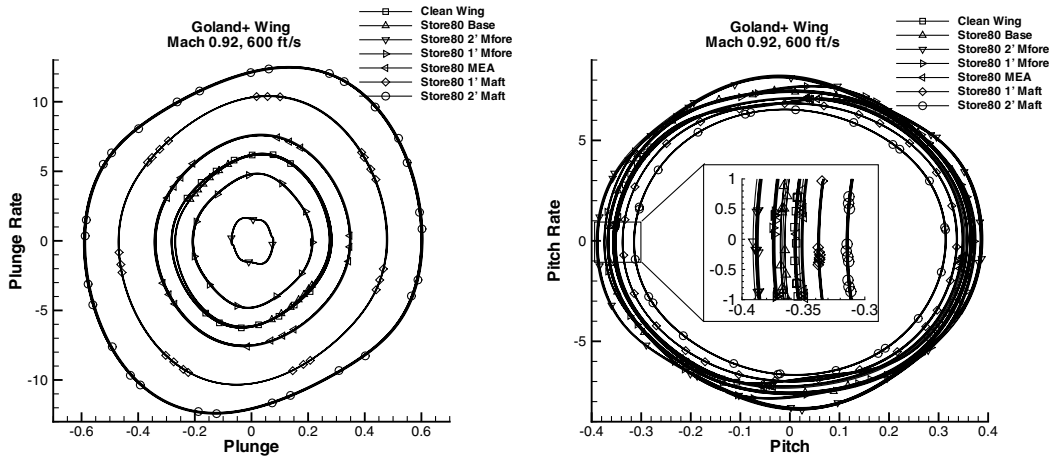

a) Plunge Phase Plot (Wing Tip) **b) Pitch Phase Plot (Wing Tip)**

Fig. 15 Phase plots for store point mass at 80% half-span.

VI. Goland+ Wing with Tip-Store Results

A tip store affected the circulation of the fluid around the wing tip and contributed to store forces, but it did not interfere with the airflow on the bottom of the wing. Adding a tip store increased the mode 1 and mode 2 responses. Like the underwing stores, the tip store primarily contributed to force in mode 3 where the tip store was responsible for 4.8% of the total mode 3 force. However, the total force in mode 3 decreased by 6.63% from that of the clean wing. Adding the tip store increased C_L by 5.06% and the tip angle of attack by 1.43%. Unlike the underwing store, the mode 1 response for the tip store oscillates about zero instead of about a negative value, the same as the clean wing. These changes resulted in the amplitudes of the motion growing faster than the clean wing and reaching LCO more quickly. The tip store increased the mode 1 amplitudes which increased the amount of bending.

The tip-store aerodynamic shape (but not the tip mass in the structural model) was shifted 2 ft (0.6096 m) fore and aft. When the tip store was moved forward, the motion damped out. Analysis showed that the flow around the tip of the wing was very sensitive to the presence of a store. Moving the tip store forward appeared to prevent the energy from flowing into the wing because mode 1 and mode 2 did not couple into a single-degree-of-freedom flutter mode, but remained independent. Unlike the LCO cases, store forces also directly correlated with modal response with mode 1 and mode 2 being the dominant force contributors. Moving the tip store aft resulted in an LCO state with a similar twist and greater plunge compared to the centered store LCO. In this case, mode 1 increased greatly when the store was shifted aft. C_L, C_M, tip angle of attack, and the modal forces all increased slightly. Mode 3 decreased slightly while modes 2, 4, 5, and 6 all increased slightly. Overall, moving the tip store fore and aft showed that the wing-tip region was very sensitive to flow changes. These flow changes manifested as changes in the mode 1 response leading to damping (move tip store forward) or by increasing the amount of plunge (move tip store aft).

To amplify the effect the store forces were having on the LCO, the store forces were magnified by ± 5 before being transferred into the structural model. Magnifying the loads in this manner affected the LCO (Fig. 9). Tip stores have the same effects as underwing stores: magnifying the bending force on the wing and increasing the LCO amplitude. The same effect was seen when the tip-store diameter was increased to 10 in. (0.254 m). As can be seen in Fig. 10, the large-diameter tip store produced a higher amplitude LCO. The large tip store contributed 9% of mode 3 forces. Unlike the underwing stores, this was a significant fraction of the total forces on the wing. The store basically acted as an extension of wing area, increasing the bending forces on the wing and increasing the LCO amplitude.

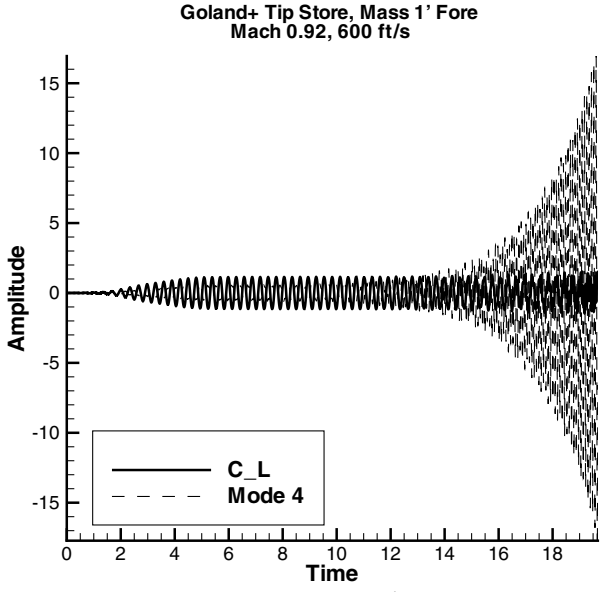

Fig. 16 Amplitudes for point mass 1′ fore of EA at tip.

To examine the effect of tip-store mass position on LCO as opposed to store aerodynamics, inertial forces were added to the store aerodynamic forces. The 5 in. (0.127 m) diameter tip store was run with a store mass located −2 ft (−0.6096 m), −1 ft (−0.3048 m), 0 ft (0.0 m), 1 ft (0.3048 m), and 2 ft (0.6096 m) in the x direction (streamwise direction) from the elastic axis. When the mass was added at the wing tip on the elastic axis, mode 6 began to grow at 2.5 s and led to divergent flutter. When the mass was added aft of the elastic axis, all of the modes, except for mode 2, began to grow which led to divergent flutter. When the mass was added forward of the elastic axis, it appeared that a coupled LCO response was obtained with mode 2 being increasingly dominant the further forward the mass was moved. However, at approximately 10 s, mode 4 rapidly began to grow leading to divergent flutter (Fig. 16). Adding inertia forces resulted in a larger aeroelastic effect than adding store aerodynamics, at least for the store geometries considered herein. Adding store aerodynamics increased the amplitude of C_L by 4.6%. Adding inertia forces at the tip in addition to the store aerodynamics led to divergence.

VII. Conclusions

The aerodynamic nonlinearity responsible for LCO of the Goland+ clean wing at Mach 0.92, 600 ft/s (182.88 m/s) was analyzed. The LCO consisted of a nearly in-phase coupling of mode 1 and mode 2, which produced a single-degree-of-freedom, torsional motion, with an axis of rotation running from the elastic axis at the root of the wing, to a point slightly forward of the leading edge at the tip of the wing. For LCO to exist, a nonlinearity must have been present to provide the quenching mechanism that limited the amplitude of the oscillations. For the Goland+ wing, the only nonlinearity present was shock motion and the appearance/disappearance of shocks. Flow separation and structural nonlinearity were not modeled. For this wing, as the oscillations grew, there was a transition from a Tijdeman type-A shock motion [4], to a Tijdeman type-B shock motion [4] in the inboard 50% span, while the shock motion in the outboard 50% span remained type-A. The type-B shock motion limited the flow of energy from the fluid into the structure and changed the amplitude growth from an exponential growth to a linear growth. This type-B motion continued to gain strength until it consisted of an appearing and disappearing shock at the trailing edge, with no observable fore/aft motion. Two additional quenching mechanisms later appeared in the outboard 50% span, which further limited the amplitude growth and led to LCO. The first was a strong, trailing-edge shock that moved fore and aft, and the second was a strong, lambda shock that ran from the leading edge of the wing near the tip, to the normal shock on the trailing edge. The combination of type-B shock motion, lambda shock motion, and the motion of the normal shock at the trailing edge were responsible for limiting the energy flow from the fluid to the structure resulting in LCO.

Aerodynamic store shapes were added to the coarse Goland+ grid at different spanwise locations to determine how store aerodynamics affect LCO. It was found that aerodynamic store shapes affect LCO in two ways: by interfering with the flowfield on the wing surface and by adding loads into the structure. Underwing stores interfered with the airflow on the lower surface of the wing, diminishing LCO amplitudes. On the other hand, the transfer of store loads into the wing structure increased LCO amplitudes for both tip stores and underwing stores. Underwing stores also led to a negative offset of the amplitudes of the primary bending mode by shifting the static aeroelastic solution. The addition of stores did not affect the LCO frequency, which was always approximately 3.3 Hz. In addition to the negative offset, underwing stores decreased the mode 1 amplitudes, which decreased the amount of bending. Tip stores increased the mode 1 amplitudes, which increased the amount of bending.

When simulating LCO, modeling the store shape is important if the store is large, such as an external fuel tank, or if the forces on the store are large. If the store is located where it will experience large motions, it is also important to include the store in the simulation. If

the store is small and inboard where the motions are small, it can most likely be safely ignored.

Acknowledgments

This work was funded by the Multidisciplinary Technologies Center, Air Force Research Laboratory (AFRL), Air Vehicles Directorate. The authors would like to thank Robert Canfield at AFIT, Oddvar Bendiksen at UCLA, and Rich Snyder at AFRL for their advice. The authors would also like to thank the Mississippi State University Engineering Research Center for the use of their grid generation software, SolidMesh.

References

[1] Bunton, R. W., and Denegri, C. M., Jr., "Limit Cycle Oscillation Characteristics of Fighter Aircraft," *Journal of Aircraft*, Vol. 37, No. 5, Sept.–Oct. 2000, pp. 916–918.

[2] Meijer, J. J., and Cunningham, A. M., Jr.,"Development of a Method to Predict Transonic Limit Cycle Oscillation Characteristics of Fighter Aircraft," *Transonic Unsteady Aerodynamics and Aeroelasticity*, CP-507, AGARD, 1992, pp. 23-1–23-21.

[3] Dowell, E. H., and Tang, D., "Nonlinear Aeroelasticity and Unsteady Aerodynamics," *AIAA Journal*, Vol. 40, No. 9, Sept. 2002, pp. 1697–1707.

[4] Tijdeman, H., and Seebass, R., "Transonic Flow Past Oscillating Airfoils," *Annual Review of Fluid Mechanics*, Vol. 12, Dec. 1980, pp. 181–222.

[5] Bendiksen, O., "Transonic Limit Cycle Flutter/LCO," AIAA, Paper 2004-1694, 2004.

[6] Janardhan, S., Grandhi, R. V., Eastep, F., and Sanders, B., "Parametric Studies of Transonic Aeroelastic Effects of an Aircraft Wing/Tip Store," *Journal of Aircraft*, Vol. 42, No. 1, Jan.–Feb. 2005, pp. 253–263.

[7] Beran, P., Khot, N., Eastep, F., Snyder, R., and Zweber, J., "Numerical Analysis of Store-Induced Limit-Cycle Oscillation," *Journal of Aircraft*, Vol. 41, No. 6, Nov.–Dec. 2004, pp. 1315–1326.

[8] Geuzaine, P., Brown, G., Harris, C., and Farhat, C., "Aeroelastic Dynamic Analysis of a Full F-16 Configuration for Various Flight Conditions," *Journal of Aircraft*, Vol. 41, No. 3, March 2003, pp. 363–371.

[9] Melville, R., "Nonlinear Mechanisms of Aeroelastic Instability for the F-16," AIAA, Paper 2002-0871, 2002.

[10] Melville, R., "Aeroelastic Instability of Tactical Aircraft in Nonlinear Flow Regimes," AIAA Paper 2002-2970, 2002.

[11] Denegri, C. M., Dubben, J. A., and Maxwell, D. L., "In-Flight Wing Deformation Characteristics During Limit-Cycle Oscillations," *Journal of Aircraft*, Vol. 42, No. 2, March–April 2005, pp. 500–508.

[12] Kim, D.-H., Park, Y.-M., Lee, I., and Kwon, O. J., "Nonlinear Aeroelastic Computations of a Wing/Pylon/Finned-Store Using Parallel Computing," *AIAA Journal*, Vol. 40, No. 1, Jan. 2005, pp. 53–62.

[13] Parker, G., Maple, R., and Beran, P., "The Role of Viscosity in Store-Induced Limit-Cycle Oscillation," AIAA, Paper 2005-1916, 2005.

[14] Parker, G., Maple, R., and Beran, P., "The Role of Store Aerodynamics in Store-Induced Limit-Cycle Oscillation," IFASD Paper IF-077, 2005.

[15] Hughes, T. J. R., *The Finite Element Method—Linear Static and Dynamic Finite Element Analysis*, Prentice_Hall, Inc., Englewood Cliffs, NJ, 1987.

[16] Smith, M. J., Hodges, D. H., and Cesnik, C. E. S., "An Evaluation of Computational Algorithms to Interface Between CFD and CSD Methodologies," Wright Laboratory, TR WL-TR-96-3055, Wright–Patterson AFB, OH, 1995.

[17] ZAERO Ver. 5.2 Theoretical Manual, 13th ed., ZONA Technology, Inc., Scottsdale, AZ, 2001.

[18] Duchon, J., "Splines Minimizing Rotation-Invariant Semi-Norms in Sobolev Spaces," *Proceedings of the Conference on Constructive Theory of Functions of Several Variables*, edited by W. Schempp, and K. Zeller, Springer–Verlag, Berlin, 1977, pp. 85–100.

[19] Harder, R. L., and Desmarais, R. N., "Interpolation Using Surface Splines," *Journal of Aircraft*, Vol. 9, No. 2, Feb. 1972, pp. 189–191.

[20] Snyder, R., Scot, J., Khot, N., Beran, P., and Zweber, J., "Preditions of Store-Induced Limit-Cycle Oscillations Using Euler and Navier-Stokes Fluid Dynamics," AIAA Paper 2003-1727, 2003.

[21] Eastep, F., and Olsen, J. J., "Transonic Flutter Analysis of a Rectangular Wing with Conventional Airfoil Sections," *AIAA Journal*, Vol. 18, No. 10, Oct. 1980, pp. 1159–1164.

[22] Goland, M., "The Flutter of a Uniform Cantilever Wing," *Journal of Applied Mechanics*, Vol. 12, No. 4, Dec. 1945, pp. 197–208.